IJTE, Vol. 13, No. 3, Winter 2026, pp. 2253-2275
Research Paper

Investigation of the Skid Resistance and Mechanical Properties of Concrete Based on Aggregate Characteristics and Cement-Paste Film Parameters

Nasrin Karimi[1], Abolfazl Arabzade[1,*], Seyedehsan Seyedabrishami[1]

Received: 2025/10/24 *Accepted: 2025/12/09*

Abstract

Maintaining pavement friction under wet conditions requires surface textures that withstand traffic-induced polishing and wear. This study evaluates how the coordinated adjustment of maximum aggregate size (MAS), aggregate gradation, packing density, paste film thickness (PFT), and mortar film thickness (MFT) governs skid resistance in slip-formed concrete pavements. Twenty mixtures were produced with Modified Fuller–Thompson exponents (0.67, 0.55, 0.45, 0.35) at MAS = 9.5, 12.5, 19, 25, and 37.5 mm. Tests included slump and Box Test, wet packing density, PFT/MFT, compressive and flexural strength, EN 1338 abrasion, ASTM E303 British Pendulum Number (BPN), Mercury Intrusion Porosimetry (MIP), and Scanning Electron Microscopy (SEM) of the Interfacial Transition Zone (ITZ). The results indicate that mixtures with MAS = 19–25 mm provided the best overall balance—higher compressive and flexural strengths, BPN typically ≥ 65, and lower abrasion rates. The study indicates that coordinating packing density with PFT and MFT—within a compatible gradation—enhances mechanical properties as well as skid resistance.

Keywords: slip-formed concrete pavement; skid resistance; abrasion resistance; MAS; packing density

* Corresponding author. E-mail: arabzade@modares.ac.ir
[1] Faculty of Civil and Environmental Engineering, Tarbiat Modares University, Tehran, Iran

1. Introduction

Maintaining sufficient pavement friction—especially in wet conditions—is critical for road safety (Nejad, Karimi and Zakeri, 2016). Prior research shows that friction is governed by two main mechanisms: adhesion, involving interfacial bonding and molecular interactions, and hysteresis, arising from the viscoelastic deformation and energy loss of the wheel's rubber as it traverses surface asperities (Zhao et al., 2023; Senthilvelan et al., 2024). The effectiveness of both mechanisms is largely dictated by microtexture (wavelengths < 0.5 mm) and macrotexture (0.5–50 mm), which together play the dominant roles in skid resistance (Hall et al., 2009; Kane and Edmondson, 2022; Senthilvelan et al., 2024).

Numerous studies have shown that factors such as aggregate mineralogy, water-to-cement ratio, admixtures (e.g., supplementary cementitious materials, fibers, rubber particles), and fine aggregate content significantly affect the skid resistance of concrete (Sherwood, no date; Hall et al., 2009; Alaskar et al., 2021; Lashari et al., 2023; Zhao et al., 2023; Senthilvelan et al., 2024). For example, Sherwood(Sherwood, no date), analyzing LTPP data, reported that increasing the volumetric fraction of fines improves pavement skid resistance. Senthilvelan et al. (Senthilvelan et al., 2024) found that control of grading and the use of harder fine aggregates enhance surface texture and sustain skid resistance over time. Likewise, Wasilewska et al.(Wasilewska, Gardziejczyk and Gierasimiuk, 2018) observed in exposed aggregate concrete (MAS = 11.2 mm) that higher contents of coarse particles (> 4 mm) yielded superior skid resistance.

packing density represents the maximum volumetric concentration of solids at an optimum water-to-solids ratio and indicates how much void space must be filled and how much excess paste or mortar remains. This excess is expressed by the paste film thickness (PFT) around fine aggregates and the mortar film thickness (MFT) around coarse aggregates. For a given paste volume, higher wet packing density reduces the void ratio and leads to a denser microstructure, which is associated with lower shrinkage and improved mechanical properties of hardened concrete, while an appropriate range of PFT and MFT is essential to ensure adequate workability in the fresh state and to avoid paste-rich surfaces that are more susceptible to abrasion and loss of skid resistance over time (Wong and Kwan, 2008, no date; Thesis, 2013; Kwan and Li, 2014; Li and Kwan, 2014; Chu, 2019).

On the other hand, aggregate packing density plays a critical role in both the fresh and hardened properties of concrete (Mamirov, no date; Schmidt and International Symposium on Ultra High Performance Concrete 1 2004 Kassel, no date; Wong and Kwan, no date; Ghoddousi, Shirzadi Javid and Sobhani, 2014; Kwan and Li, 2014; Li and Kwan, 2014; Sun et al., 2022; Liu et al., 2025). By tuning maximum aggregate size (MAS) and overall gradation, particle packing can be improved, paste demand lowered, and—consequently—workability, mechanical strength, dimensional stability, and durability enhanced. These considerations are particularly critical for "green" concrete, where reducing Portland cement content—and thus the carbon footprint—is a central goal (Wong and Kwan, no date; Fattouh et al., 2025).

no research to date has explored the contribution of an optimized combination of MAS and aggregate grading (spanning both fine and coarse fractions) on abrasion resistance and skid resistance, even though MAS and aggregate grading are key variables controlling wet packing density and, consequently, PFT and MFT in concrete mixtures.

Here, we examine how MAS and particle-size distribution (via the modified Fuller–Thompson gradation) influence workability, wet packing density, paste film thickness (PFT), and mortar film thickness (MFT), and how these, in turn, affect mechanical properties and skid resistance.

2. Materials and Methods

2.1. Raw Materials

The cement used in this research was a local Portland type II, according to the characteristics of ASTM C150 (Designation: C 150-07 Standard Specification for Portland Cement 1, no date). The physical and chemical specifications of cement are shown in Table 1. fine aggregate with a specific gravity of 2500 kg/m³, water absorption of 1.62%, and an uncompacted void content of 34% was used. Crushed gravel with five different maximum sizes of 37.5, 25, 19, 12.5, and 9.5 mm, with a specific gravity of 2560 kg/m^3, water absorption of 1.5%, and single-face crushing percentage of 67% and dual-face crushing percentage of 87%, was used as coarse aggregate. The mixing proportion of the Coarse and fine aggregates were chosen according to the modified Fuller–Thompson gradation. The Modified Fuller–Thompson gradation can be determined as (Equation(1)) (Advanced Concrete Technology, no date):

$$P = 100\left(\frac{d}{D}\right)^{n} \quad (1)$$

where P is the cumulative percentage passing through a sieve with diameter d, D is the maximum aggregate size in the mixture, and n is the gradation exponent that controls the distribution of particle sizes. In the modified version, various values of n (typically ranging between 0.1 and 0.67) are adopted to tailor the gradation for specific performance criteria. In this study, four exponent values of 0.67, 0.55, 0.45, and 0.35 were employed to generate 20 distinct aggregate gradations. The results of particle size measurement of solid materials used in this research are shown in Figure. 1. Here, A, B, C, D, and E correspond to MAS values of 37.5 mm, 25 mm, 19 mm, 12.5 mm, and 9 mm, respectively. Similarly, the numbers 1 to 4 represent Fuller–Thompson Exponent(FTE) values of 0.67, 0.55, 0.45, and 0.35, respectively. Superplasticizer (SP) based on polycarboxylic-ether, confirming ASTM C494 (Designation: C 494/C 494M-99a e1 Standard Specification for Chemical Admixtures for Concrete 1, no date) was consumed to set the required workability which is constant for all mixtures.

Table 1. Chemical and physical properties of cement

	cement
Chemical analysis %	
Silica (SiO2)	20.7
Alumina (Al2O3)	4.9
Iron oxide (Fe2O3)	3.5
Calcium oxide (CaO)	62.9
Magnesia (MgO)	1.2
Sulfur trioxide (SO3)	3.3
Sodium oxide (Na2O)	0.3
Potassium oxide (K2O)	0.6
Loss of ignition	2.3
Bogue potential compound composition, %	
Tricalcium silicate (C3S)	59
Di calcium silicate (C2S)	15
Tricalcium aluminate (C3A)	5.5
Tetra calcium aluminoferrite(C4AF)	13
Physical properties	
Specific surface, cm2/g	3175
Specific gravity	3.15
Bulk density, g/cm3	1.23

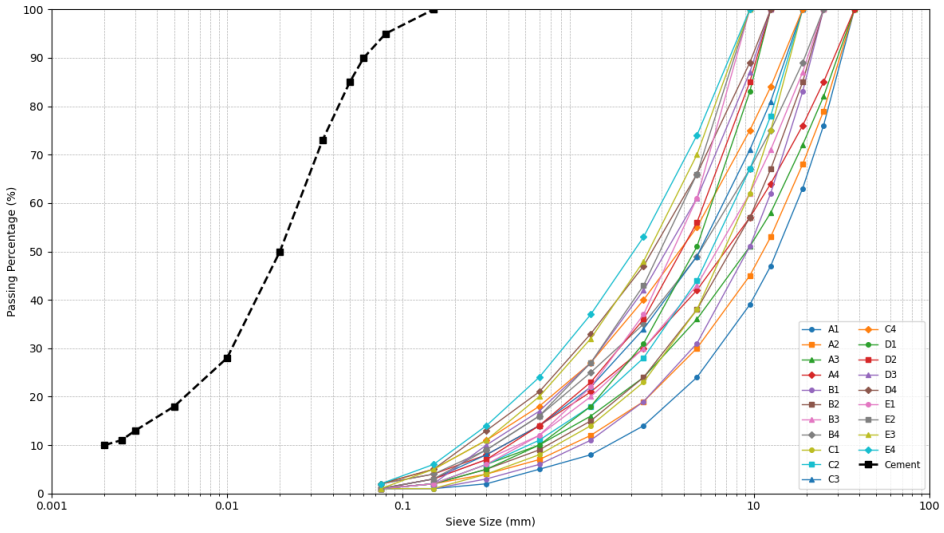

Figure 1. Individual particle size distribution of each solid material

2.2. Mixture Proportions

Minimum paste is needed to fill aggregate voids, coat particles, and lubricate the mix for the required workability. Koehler and Fowler introduced the "minimum paste theory" to establish a relationship between paste volume and concrete performance for specific aggregate systems (Koehler and Fowler, no date) .This approach was later extended to pavement concrete by Ezgi et al. (2013) and Wang et al. (2018), offering a quantitative framework to evaluate the interaction between paste and aggregate structure for enhanced performance. The method involves four key steps: (1) selecting an appropriate aggregate system to minimize voids and achieve optimal packing, (2) choosing the paste quality, including binder type and admixture dosages, (3) determining the required paste volume to fill the aggregate voids (they proposed a paste-to-voids volume ratio in the range of 125% to 175% for concrete pavements), and (4) calculating the final mixture proportions based on these parameters. This approach ensures the efficient use of materials while improving workability, strength, and durability in concrete pavements (Yurdakul et al., 2013; Wang et al., 2018).

In this research, 20 concrete mixtures were designed based on 20 distinct aggregate gradations**.** Concrete mixtures were prepared with water-to-cement ratios of 0.45 and V_{paste}/V_{voids} of 160%, where the volume of voids in the consolidated combined aggregate system was determined by ASTM C29 and ASTM C127 (Designation: C 29/C 29M-07 Standard Test Method for Bulk Density ("Unit Weight") and Voids in Aggregate 1, no date).Mixtures' compositions are listed in Table 2.

Table 2. Proportions of the components in the 20 concrete mixtures

Mixture code	MAS (mm)	FTE	V_{paste} (m^3)	V_{paste} / $V_{aggregate}$	Quantities (kg/m^3)			Super plasticizer
					cement	gravel	sand	(cement%)
1	37.5	0.67	0.281	0.403	367	1351	426	0
2		0.55	0.257	0.356	335	1285	551	0
3		0.45	0.231	0.309	302	1216	648	0.6
4		0.35	0.213	0.278	278	1128	816	0.7
5	25	0.67	0.282	0.403	367	1224	550	0.1
6		0.55	0.257	0.356	335	1136	697	0.1
7		0.45	0.257	0.356	335	1044	787	0.2

Mixture code	MAS (mm)	FTE	V_{paste} (m^3)	V_{paste} / $V_{aggregate}$	Quantities (kg/m^3)			Super plasticizer
					cement	gravel	sand	(cement%)
8		0.35	0.24	0.325	313	954	917	0.3
9		0.67	0.289	0.419	377	1086	666	0.3
10	19	0.55	0.266	0.372	346	1013	796	0.4
11		0.45	0.257	0.356	335	932	896	0.5
12		0.35	0.24	0.325	313	841	1028	0.5
13		0.67	0.282	0.403	367	865	901	0.3
14	12.5	0.55	0.282	0.403	367	776	988	0.3
15		0.45	0.266	0.372	346	703	1099	0.4
16		0.35	0.257	0.356	335	619	1202	0.8
17		0.67	0.297	0.435	387	672	1051	0.5
18	9.5	0.55	0.282	0.403	367	598	1162	0.5
19		0.45	0.274	0.387	357	533	1245	0.8
20		0.35	0.266	0.372	346	467	1330	0.8

3. Methodology

3.1. Workability and Density of Fresh Mixtures

The workability tests were conducted according to the ASTM C143 and Cook et al. (2014) (International and indexed by mero, no date; Cook, Ley and Ghaeezadah, 2014).The tests included the slump test and box test to evaluate fresh concrete performance. In slip-form concrete pavement construction, the box test and the slump test serve as complementary methods for evaluating fresh concrete consistency. While the slump test provides a general indication of workability, The box test offers a more accurate assessment of shape stability and edge retention by simulating compaction and form removal of slip-form paving. In the box test, after vibration and removal of the forms, the exposed surface and edges of the concrete are visually evaluated on a 1–4 rating scale based on the percentage of surface voids and the ability of the mix to retain its edges. Mixtures with less than about 10% and 30% surface voids are assigned ratings of 1 and 2, respectively, whereas mixtures with higher surface void contents and noticeable loss of edge stability are rated 3 or 4 and are considered unsuitable for slip-form paving. Also, fresh mixture density was tested according to the ASTM C138 (Standard Test Method for Density (Unit Weight), Yield, and Air Content (Gravimetric) of Concrete 1, no date).

3.2. Measurement of Packing Density, PFT, and MFT

A method for determining packing density, known as the wet packing method and initially developed by Wong and Kwan (Wong and Kwan, 2008), was adopted in this study to assess the actual packing density of the concrete mixtures. The measurement procedure was conducted as follows: After mixing, the fresh concrete was transferred into a cylindrical container with dimensions of 180 mm in height and 160 mm in diameter. The mass and volume of the mixture within the container were recorded as M and V, respectively. For mixtures comprising multiple constituent materials, the volume of solids contained in the container (Vc) was calculated using Equation (2):

$$V_C = \frac{M}{\rho_w u_w + \rho_g R_g + \rho_s R_s + \rho_c R_c + \rho_m R_m} \quad (2)$$

where ρ_w is the water density, u_w is the volumetric ratio of water to the solid material, and ρ_g, ρ_s, ρ_c, and ρ_m are the gravel, sand, cement, and cement replacement admixtures, respectively. Moreover, R_g, R_s, R_c and R_m are the ratios of gravel, sand, cement, and cement replacement admixture volume to the total solid

materials, respectively. The variable values are presented in Table 3. Having V_C And V, the packing density (φ) can be calculated using Equation (3):

$$\varphi = \frac{V_C}{V} \quad (3)$$

Table 3. The variable values for the packing density calculation

Variables	Value (kg/m^3)
ρ_w	1000
ρ_g	2560
ρ_s	2500
ρ_c	3150

The PFT is defined as the average thickness of the paste coating on the surface of aggregate particles larger than 75 μm. It is calculated as the ratio of excess paste volume (which includes water, cement, and aggregate fines smaller than 75 μm) to the specific surface area of the coarser aggregate particles (> 75 μm) that can be calculated from its particle size distribution. The excess paste volume (u'_p) is obtained by subtracting the minimum voids ratio from the total paste ratio of the mixture, as follows (Equation (4)-(6)) (Kwan and Li, 2014):

$$u_{a,min} = \frac{1 - \varphi_{a,max}}{\varphi_{a,max}} \quad (4)$$

$$u'_p = u_p - u_{a,min} \quad (5)$$

$$PFT = \frac{u'_p}{A_A} \quad (6)$$

Where:

- $\varphi_{a,max}$: Wet packing density of aggregate particles > 75 μm
- $u_{a,min}$: Minimum voids ratio
- u_p: Paste ratio (volume of paste to solid volume of aggregate > 75 μm)
- A_A: Specific surface area of aggregate particles > 75 μm
- PFT: Paste film thickness

Similarly, the MFT is defined as the average thickness of mortar surrounding aggregate particles larger than 1.2 mm. Mortar is considered the combination of paste and fine aggregates smaller than 1.2 mm. The excess mortar volume (u'_m) is calculated similarly to that of paste, using the packing density of aggregate particles larger than 1.2 mm. MFT can be obtained from Equations (7), (8), and (9)(Kwan and Li, 2014):

$$u_{c,min} = \frac{1 - \varphi_{c,max}}{\varphi_{c,max}} \quad (7)$$

$$u'_m = u_m - u_{c,min} \quad (8)$$

$$MFT = \frac{u'_m}{A_C} \quad (9)$$

where

- $\varphi_{c,max}$: Wet packing density of aggregate particles > 1.2 mm
- $u_{c,min}$: Minimum voids ratio
- u_m: Mortar ratio (volume of mortar to solid volume of aggregate > 1.2 mm)
- A_C: Specific surface area of aggregate particles > 1.2 mm
- MFT: Mortar film thickness

3.3. Mechanical Properties Tests

Compressive strength and flexural strength tests of samples were done according to ASTM C39, ASTM C78 and ("Test Method for Flexural Strength of Concrete (Using Simple Beam With Center-Point Loading)," 2016; Standard Test Method for Compressive Strength of Cylindrical Concrete Specimens 1, no date).

3.4. Abrasion Test

The abrasion test was conducted on cubic specimens using the wide wheel abrasion method by EN 1338 standard (Figure. 2) (no date).

Figure 2. Wide wheel test machine

3.5. Skid Resistance Test

The British Pendulum Test was employed to assess skid resistance of concrete spacemens surfaces. The British Pendulum Test (ASTM E303) is a widely used method for evaluating the skid resistance of flooring and road surfaces ("Test Method for Measuring Surface Frictional Properties Using the British Pendulum Tester," 2008). It utilizes a pendulum device to measure the dynamic coefficient of friction (British Pendulum Number; BPN) by impacting a rubber slider against the test surface.

3.6. Microstructure Tests

- MIP

Total porosity and pore size distribution of mixtures were determined using the Mercury Intrusion Porosimetry (MIP) method, applying a maximum pressure of 210 MPa. Concrete fragments approximately 5 mm in diameter, free of coarse aggregate, were extracted on day 28 for analysis.

- Scanning Electron Microscope (SEM)

scanning electron microscope was used to assess the effect of aggregate gradation on the internal microstructure of concrete specimens, and representative images were selected to measure the average thickness of the ITZ.

4. Test Results

4.1. Workability of the Fresh Mixtures

Slump and box test results are presented in Table 4.

Table 4. Slump and box test results

Mixture code	Box Test rank	Slump (mm)
1	4	70
2	3	50
3	3	50
4	3	30
5	2	30
6	2	30
7	2	30
8	2	40
9	2	40
10	2	30
11	1	50
12	1	30
13	1	40
14	1	30
15	1	30
16	1	30
17	1	30
18	1	30
19	1	30
20	1	30

Despite acceptable slump, mixtures with a MAS of 37.5 mm were hard to place and compact: they repeatedly lost shape and edge stability and failed the Box Test (Figure. 3). These observations indicate that slump alone is insufficient for evaluating suitability of concrete mixtures for slip-form paving. The Box Test should be used alongside slump as the more reliable indicator of mix stability and workability under such conditions.

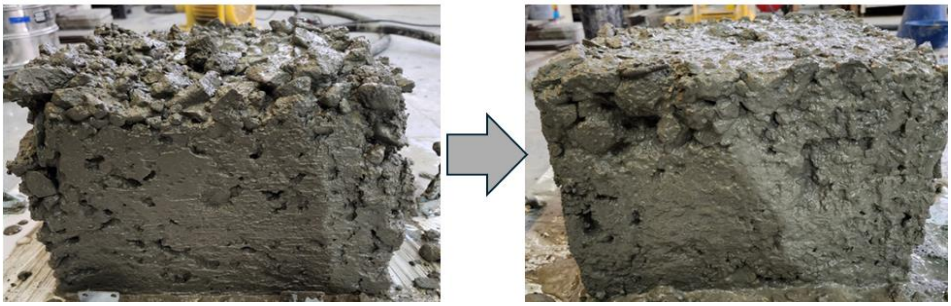

Figure 3. Concrete mix with 37.5 mm maximum aggregate size (MAS) failing the Box Test after two attempts due to poor consistency and edge stability

4.2. Mechanical Properties of Mixtures

The mechanical properties of the mixtures are presented in Figure. 4 and Figure.5. The highest compressive strength (46 MPa) was obtained at a MAS of 19 mm, while the lowest (30 MPa) was observed at MAS of 37.5 mm. Similarly, the highest flexural strength (7.3 MPa) was

recorded at MAS values of 19 mm and 25 mm, suggesting favorable mechanical performance at these sizes. In contrast, the lowest values for these properties were observed at MAS values of 9.5 and 37.5 mm.

The compressive strength increases with the increase of FTE. The increases in compressive strength between the finest-graded and coarsest-graded mixes for MAS 9.5, 12.5, 19, 25, and 37.5 were 22%, 31%, 21%, 21%, and 8%, respectively. The explanation is that finer aggregate gradation increases the surface area of the particles, thereby in a constant Vpast/Vvoid, leading to a weaken interfacial transition zone (ITZ) in concrete based on lower thickness of paste around aggregates. This result can lower its compressive strength. In contrast, coarser aggregate gradation result in a strength ITZ volume, helping improve the concrete's mechanical properties(Meddah, Zitouni and Belâabes, 2010; Wang et al., 2024).

The flexural strength decreases with increasing FTE. The decreases in flexural strength between the finest-graded and coarsest-graded mixes for MAS 9.5, 12.5, 19, 25, and 37.5 were 24%, 28%, 16%, 25%, and 19%, respectively. Finer aggregate grading reduces the cement-paste film thickness and decreases the interparticle spacing, thereby enhancing mechanical interlock and friction between grains. Closely spaced fines deflect and branch cracks, lengthening their path and increasing fracture energy. Consequently, concrete containing finer aggregates exhibits higher flexural strength (Sun et al., 2023).

In all FTEs, with the increase of MAS, the compressive strength and flexural strength increase first and then decrease) intermediate MAS values (≈19–25 mm) consistently delivered the best overall balance (. This result is consistent with those of Ref. (Wang et al., 2024), which demonstrated that as the MAS increases from 19 to 26.5 mm, the thickness of the interfacial transition zone (ITZ) decreases, thereby enhancing the bond between the aggregates and the cement matrix. However, beyond this range, the ITZ thickness increases again, leading to a reduction in mechanical properties

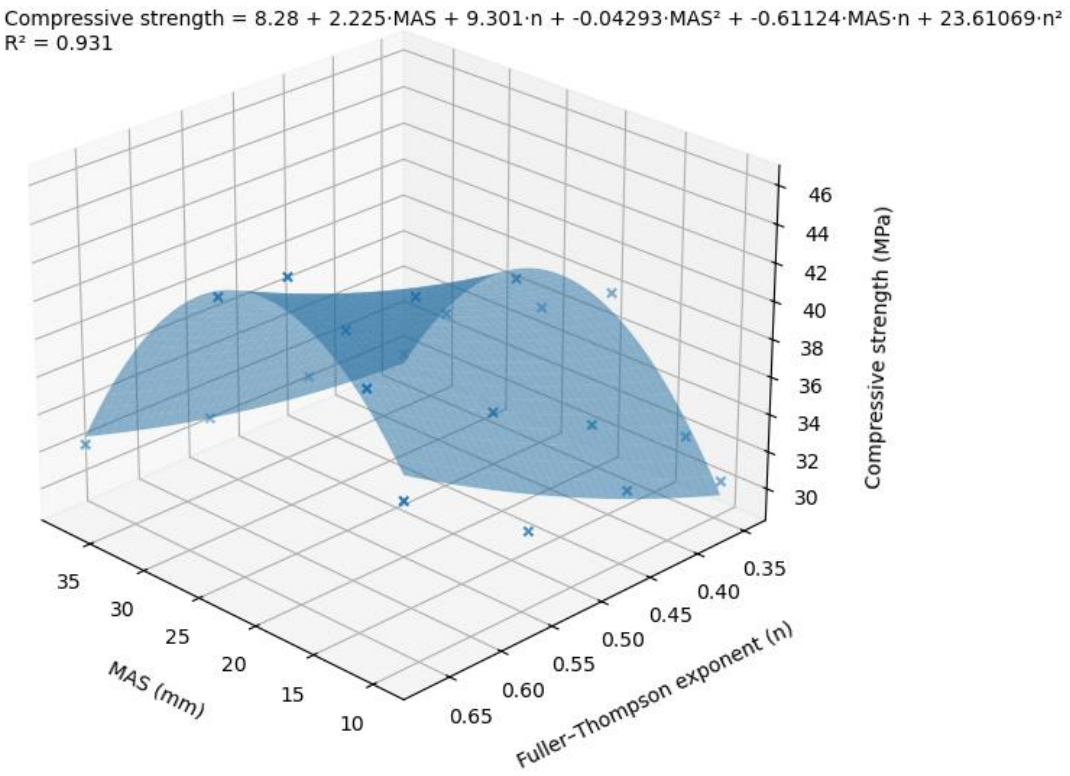

Figure 4. Compressive strength of concrete mix against FTE at different MASs

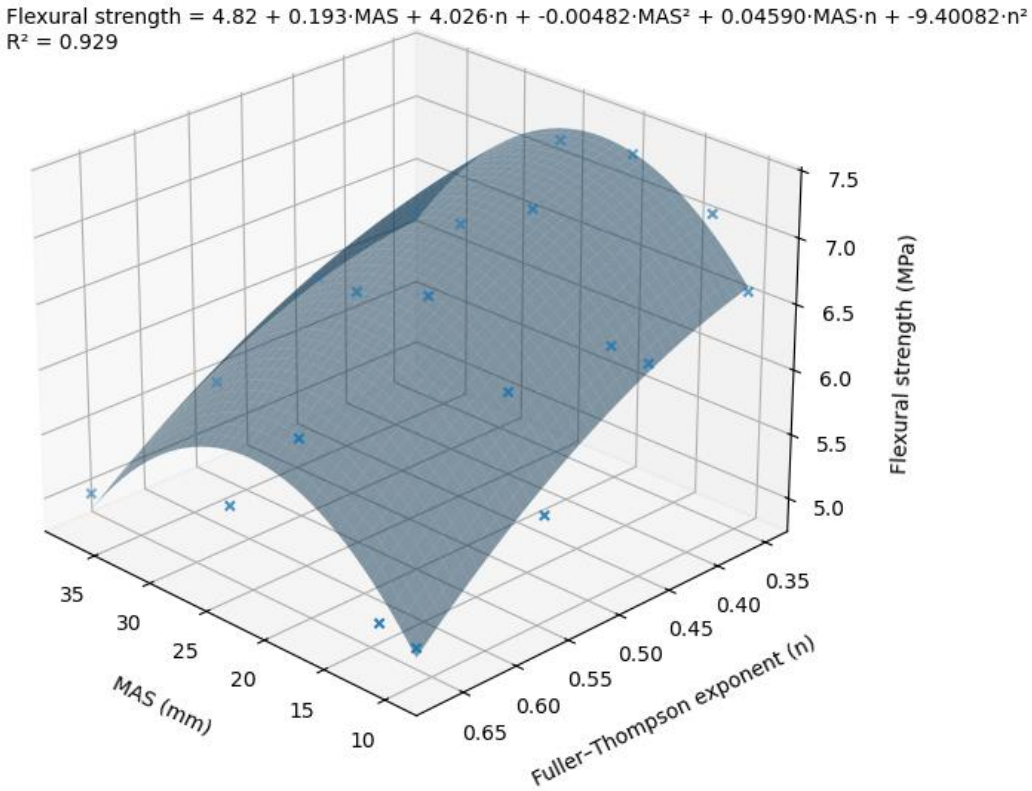

Figure 5. Flexural strength of concrete mix against FTEat different MASs

4.3. Packing Density, PFT, and MFT

The total wet packing density of the concrete mixtures (Figure. 6) ranged from 0.829 to 0.867, with the highest value observed at MAS = 37.5 mm and the lowest at MAS = 12.5 mm. Overall, the packing density increased with larger maximum aggregate size (MAS) due to the broader particle size range and the more efficient void filling by finer particles (Thesis, 2013).

Within each MAS group, finer gradations produced higher packing densities, with relative increases of 1.8%, 1.5%, 1.3%, 0.7%, and 0.2% for MAS values of 37.5, 25, 19, 12.5, and 9.5 mm, respectively. For larger MAS values (19, 25 and 37.5 mm), the improvement in packing density with finer gradation was mainly attributed to the enhanced void-filling effect, where the finer particles effectively occupied the interstitial voids between coarse aggregates, leading to a denser particle arrangement. In contrast, for the smaller MAS values (9.5 and 12.5 mm), the narrow particle size range and the already high proportion of fine particles resulted in an almost constant packing density regardless of gradation refinement, as the mixtures were already close to their maximum compactness.

To relate the compaction of the aggregate skeleton to that of the whole concrete, the total wet packing density of the mixes was plotted against the aggregate dry packing density (ranged from 0.71 to 0.81) obtained from ASTM C29 (Figure. 7). A quadratic fit captured the overall trend of the data. The analysis yielded a coefficient of determination of R^2=0.837, indicating a strong positive association between aggregate packing and the total packing density of the concrete. Although the number of data points is limited, the best-fit curve may not be generally applicable to all concrete mixes. The wet packing density results for aggregate particles larger than 75 µm and those larger than 1.2 mm, along with the corresponding PFT and MFT values for all 20 mixtures, are presented in Tables 5 and 6, respectively.

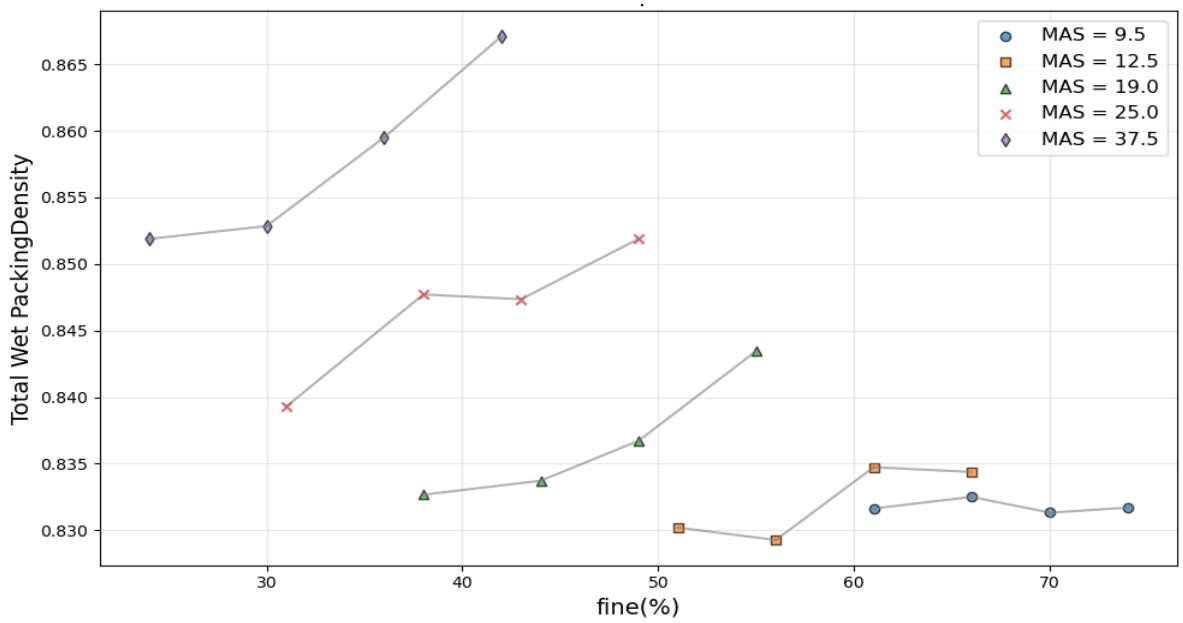

Figure 6. Total wet packing density of concrete mixtures versus fine aggregate content for different MAS values

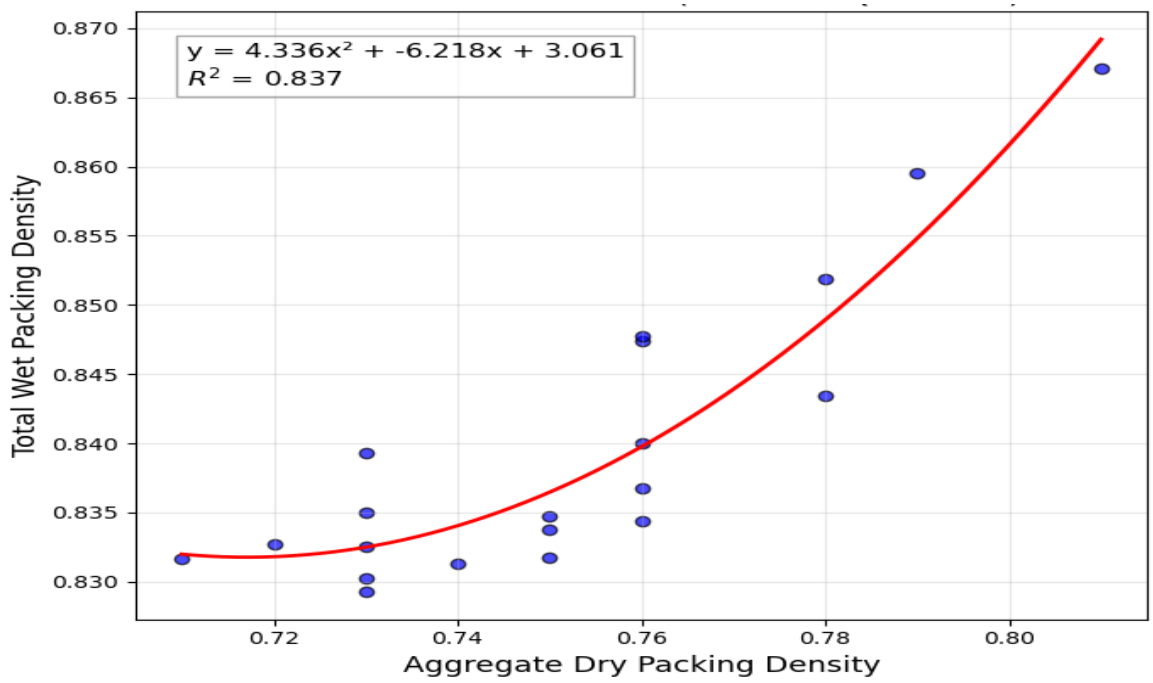

Figure 7. Total wet packing density versus aggregate dry packing density

For aggregate particles >75 μm and >1.2 mm, wet packing densities ranged between 0.814–0.852(4.6% change) and 0.796–0.851 (6.9% change), respectively. Despite the narrow density ranges, significant effects were noted in film-related parameters: excess paste ratio increased by 111%, and excess mortar ratio by 170%. These changes are attributed to the reductions in specific surface area caused by increasing MAS and FTE, which influenced coating efficiency. Consequently, PFT varied from 20 to 123 μm (increasing with MAS and FTE). Also, MFT ranged from 0.35 to 0.53 mm (increasing as FTE decreased), revealing a consistent relationship with MAS and FTE variations.

Table 5. Paste film thickness (PFT, µm) of the concrete mixtures

Mix No.	Packing density of aggregate particles > 75 μm	Paste ratio	Excess paste ratio	Surface area of aggregate particles >75μm (m^2/m^3)	PFT (μm)
1	0.85	0.403	0.224	1819	123
2	0.845	0.356	0.173	2524	69
3	0.852	0.311	0.137	3286	42
4	0.851	0.28	0.106	4170	25
5	0.836	0.408	0.211	2359	90
6	0.84	0.36	0.17	3130	54
7	0.84	0.365	0.174	4193	42
8	0.837	0.336	0.141	4787	29
9	0.83	0.42	0.214	2925	73
10	0.826	0.373	0.164	3676	45
11	0.829	0.358	0.153	4701	32
12	0.823	0.358	0.143	5805	25
13	0.823	0.405	0.19	3670	52
14	0.822	0.405	0.188	4768	39
15	0.82	0.374	0.154	5376	29
16	0.82	0.36	0.141	6643	21
17	0.817	0.437	0.214	4305	50
18	0.825	0.406	0.194	5548	35
19	0.814	0.39	0.163	6370	26
20	0.817	0.375	0.152	7593	20

Table 6. Mortar film thickness (MFT, mm) of the concrete mixtures

Mix No.	Packing density of aggregate particles >1.2 mm	mortar ratio	Excess mortar ratio	Surface area of aggregate particles >1.2 mm (m^2/m^3)	MFT (mm)
1	0.845	0.525	0.342	740	0.46
2	0.844	0.541	0.356	813	0.44
3	0.848	0.558	0.38	887	0.43
4	0.851	0.617	0.443	964	0.46
5	0.83	0.577	0.373	922	0.4
6	0.836	0.595	0.4	1007	0.4
7	0.831	0.695	0.492	1066	0.46
8	0.831	0.767	0.564	1123	0.5
9	0.821	0.65	0.432	1066	0.4
10	0.819	0.673	0.453	1139	0.4
11	0.819	0.739	0.518	1228	0.42
12	0.813	0.858	0.629	1335	0.47
13	0.815	0.711	0.485	1370	0.35
14	0.809	0.822	0.586	1412	0.42
15	0.811	0.879	0.646	1505	0.43
16	0.804	1.024	0.781	1536	0.51
17	0.812	0.839	0.59	1565	0.39
18	0.808	0.922	0.684	1637	0.42
19	0.799	1.04	0.79	1684	0.47
20	0.796	1.178	0.921	1739	0.53

4.4. Abrasion Resistance

Abrasion resistance was evaluated according to EN 1338 by measuring groove widths after five staged revolutions (200–1000 rev). For each mixture, a mean abrasion rate (mm·rev^{-1}) was calculated. Figure. 8 displays the abrasion rate of concrete mixtures at varying MAS values. The data highlights a general trend where abrasion rates decrease as MAS increases until MAS of 25 mm and then increase again. Mixes with MAS 25 mm and MAS 19 mm show consistently lower abrasion rates compared to mixtures with smaller aggregates. For instance, Mix 7 (with MAS 25 mm) shows the lowest abrasion rate (0.011 mm/r), while Mix 20 (with MAS 9.5 mm) exhibits the highest abrasion rate (0.019 mm/r). Interestingly, as the FTE (shown by different colors in the graph) increase, the abrasion rate decreases for MAS 9.5 mm, 12.5 mm and 19 mm, but this trend converse in larger aggregate sizes. These findings indicate that the better abrasion resistance of mixtures with MAS 19–25 mm is primarily associated with the development of an optimal microstructural density and strong aggregate–matrix bonding, which enhance load transfer efficiency and minimize surface abrasion(Pei et al., 2025).

4.5. British Pendulum Test results

The results of the British Pendulum Test presented in Figure 9.

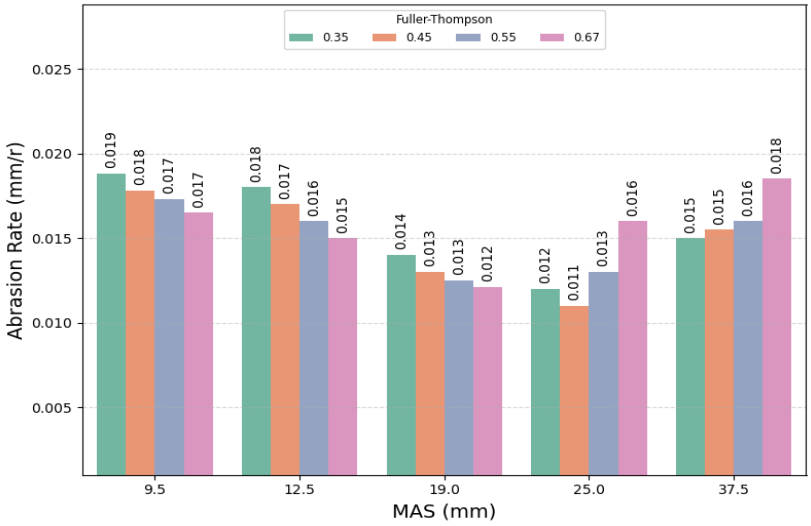

Figure 8. Abrasion rate vs maximum aggregate size (MAS) for different Fuller–Thompson exponents (FTE)

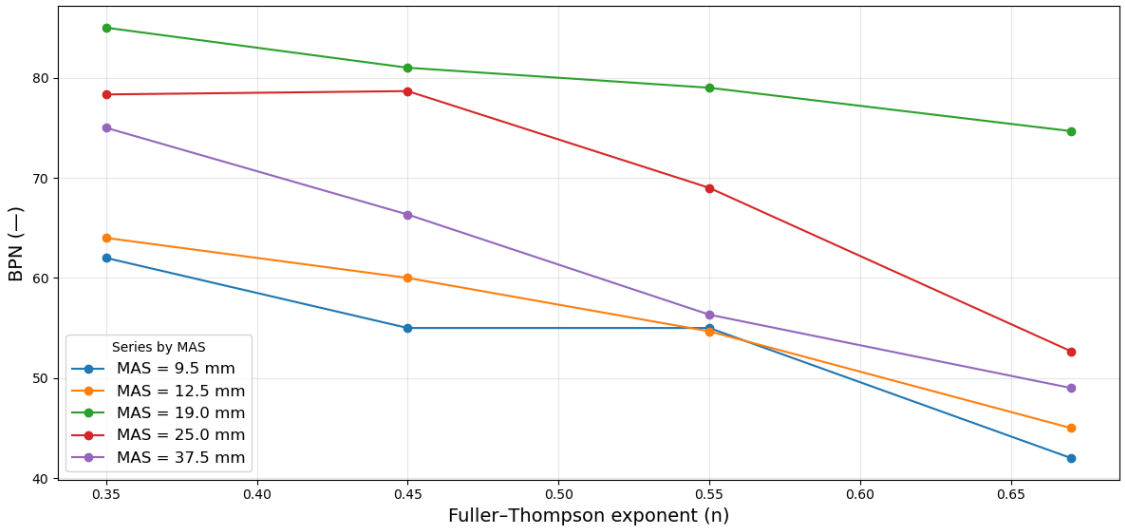

Figure 9. BPN trend vs FTE for different MAS

Results from the British Pendulum Test (BPT), spanned BPN = 42–85 across the twenty mixes. Mixtures with MAS = 19 mm (Mixes 9–12) recorded the highest BPN (≈75–85), followed by MAS = 25 mm (Mixes 5–8; ≈52–78). In contrast, MAS = 9.5 mm (Mixes 17–20) and 12.5 mm (Mixes 13–16) produced lower ranges (≈42–62 and ≈45–64), while 37.5 mm (Mixes 1–4) fell between ≈49–75. During placement, coarse particles settle and mortar rises; thus the exposed surface is predominantly mortar (≈85–90%), so the distribution of fines within the surface mortar largely governs microtexture (Zhao et al., 2023). Consistent with this mechanism, coarsening the gradation (higher Fuller–Thompson exp) systematically reduced BPN within each MAS class. For context, BPN ≥ 65 is a commonly cited threshold for road-surface skid resistance in general roadway safety standards(Sabey, 1963) Therefore, the results indicate that only mixtures 3, 4, and 6–12, which yielded BPN values between 66 and 85, exceed this threshold.

4.6. Microstructure

4.6.1. MIP Results

Numerous studies have shown that total porosity alone cannot precisely predict concrete's macroscopic properties, as these also depend on pore morphology, size and distribution. Even at identical porosity levels, significant variations in concrete characteristics are observed. Wu further classified pores into innocuous (<20 nm), less harmful (20–50nm), harmful (50–200nm), and more dangerous (>200 nm). This classification highlights that refining the pore structure by increasing less harmful pores and reducing larger, more detrimental pores can enhance concrete strength despite higher overall porosity (Xiao et al., 2023).

In order to more microstructural assessment, Mercury Intrusion Porosimetry (MIP) was performed on mixtures 3, 7, 11, 15, and 19 mm. Table 7 summarizes the results, including total porosity and average pore diameter for each mixture. Additionally, the percentages of innocuous, less harmful, harmful, and more harmful pores constituting the pore structure of each mixture, as determined by the MIP tests, are also provided.

Table 7. MIP Results for Concrete Mixtures with different MAS & FTE of 0.45

Mix no	Total porosity (%)	Average pore diameter (nm)	Pores distribiution (%)			
			Innocuous (< 20 nm)	less harmful (20-50nm)	Harmful (50-200nm)	more harmful (>200 nm)
3	41.99	76.28	15	27	45	13
7	18.22	8.7	48	32	11	9
11	22.64	10.52	17	38	28	17
15	35.65	96.27	15	24	46	15
19	38.25	80.84	16	21	44	19

lts show that the total porosity of the concrete mixtures ranges from 18.22% (Mix 7) to 41.99% (Mix 3), with the average pore diameter varying from 8.7 nm (Mix 7) to 96.27 nm (Mix 15). These variations highlight significant differences in the microstructure across the mixes, influenced by the aggregate size and composition. In particular, for Mixes 15 and 19, the narrow particle-size range and the high proportion of fines result in higher total porosity and larger average pore diameters. By contrast, Mix 3 (MAS = 37.5 mm) shows larger voids and a less compact microstructure, likely due to workability, casting/placement, and compaction challenges. Consequently, Mix 3 shows higher porosity (41.99%) compared to mixes with smaller MAS.This effect leads to larger voids and a less compact microstructure. Consequently, Mix 3 shows higher porosity (41.99%) compared to mixes with smaller MAS. When comparing Mix 7 and Mix 11 (with MAS 25 mm and 19 mm), it appears that a more optimal combination of fine and coarse aggregates leads to lower porosity and smaller

average pore diameters, likely contributing to their enhanced abrasion resistance and skid resistance. The better packing and denser matrix in Mix 7 reduce the harmful pore fraction and enhance overall durability. The combined fraction of safe pores ("innocuous" + "less harmful") varies from 37% (Mix 19) to 79% (Mix 7), reflecting the presence of smaller, less penetrable pores that typically contribute to better durability. Mix 19 and Mix 15 show a lower proportion of safe pores (37% and 39%), while Mix 7 has a significantly higher fraction of safe pores (79%), followed by Mix 11 with 55% safe pores, suggesting better long-term durability.

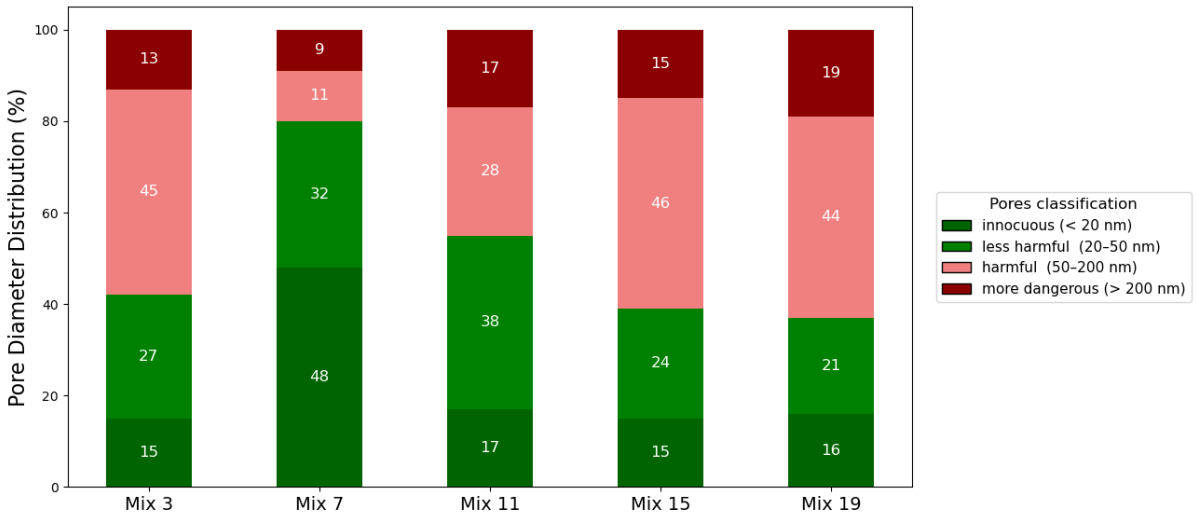

Figure 10. Pore Diameter Distribution (%)

Figureure 10 presents the pore size distribution of mixtures in table 8 based on mercury intrusion porosimetry (MIP). As observed, the proportion of harmful and more dangerous pores (with diameters exceeding 50 nm) varies considerably among the mixtures. Mix 3, Mix 15, and Mix 19 exhibit the highest share of harmful pores, exceeding 55% of total porosity, indicating a more open pore structure. Conversely, Mixes 7 and 11 show the most refined pore structure, with a combined fraction of innocuous and less harmful pores exceeding 55%, suggesting a denser microstructure. A comparison with the total porosity and average pore diameter data (Table 8) shows a consistent trend. Mixtures with higher proportions of harmful pores (Mix 3, 15, and 19) correspond to higher total porosity (41.99%, 35.65% and 38.25%) and larger average pore diameters (76.28nm, 96.27 nm and 80.84 nm, respectively).

4.6.2. SEM Results

The ITZ thickness of each mix at a FTE of 0.45 was measured (Figure. 11). The width of the ITZ may be affected by the cutting method, which could result in uneven ITZ thicknesses. Therefore, the reliability of the test results was verified using statistical methods. The average width (W_C), standard deviation (δ), and extreme values ($W_{C\ max}$ and $W_{C\ min}$) of the ITZ thicknesses are presented in Table 8.

Table 8. Statistical parameters of ITZ thickness

Mix no	W_C (µm)	δ (µm)	$W_{C,\ max}$(µm)	$W_{C,\ min}$(µm)
3	5.02	0.97	6.4	3.23
7	2.44	0.69	3.59	1.33
11	4.01	0.58	4.88	3.11
15	6.19	0.7	6.77	5.13
19	8.82	1.44	10.65	6.11

The average ITZ thicknesses for mixes 3, 7, 11, 15, and 19 were 5.02 µm, 2.44 µm, 4.01 µm, 6.19 µm, and 8.82 µm, respectively. As MAS increases, the ITZ thickness first decreases and then increases. Mix 7 (with MAS 25 mm) shows the smallest ITZ thickness of 2.44 µm,

indicating a stronger bond between the aggregate and mortar, leading to a denser interfacial zone. In comparison to Mix 7, the ITZ thicknesses for Mixes 3, 11, 15, and 19 increased by 106%, 64.6%, 153.7%, and 261.8%, respectively. This behavior aligns with previous studies (Wang et al., 2024), which showed that as MAS increases from 19 mm to 26.5 mm, the ITZ thickness decreases, improving the bond between the aggregates and the cement paste. However, beyond this range, the ITZ thickness increases again, which may reduce the mechanical properties and durability of the concrete.

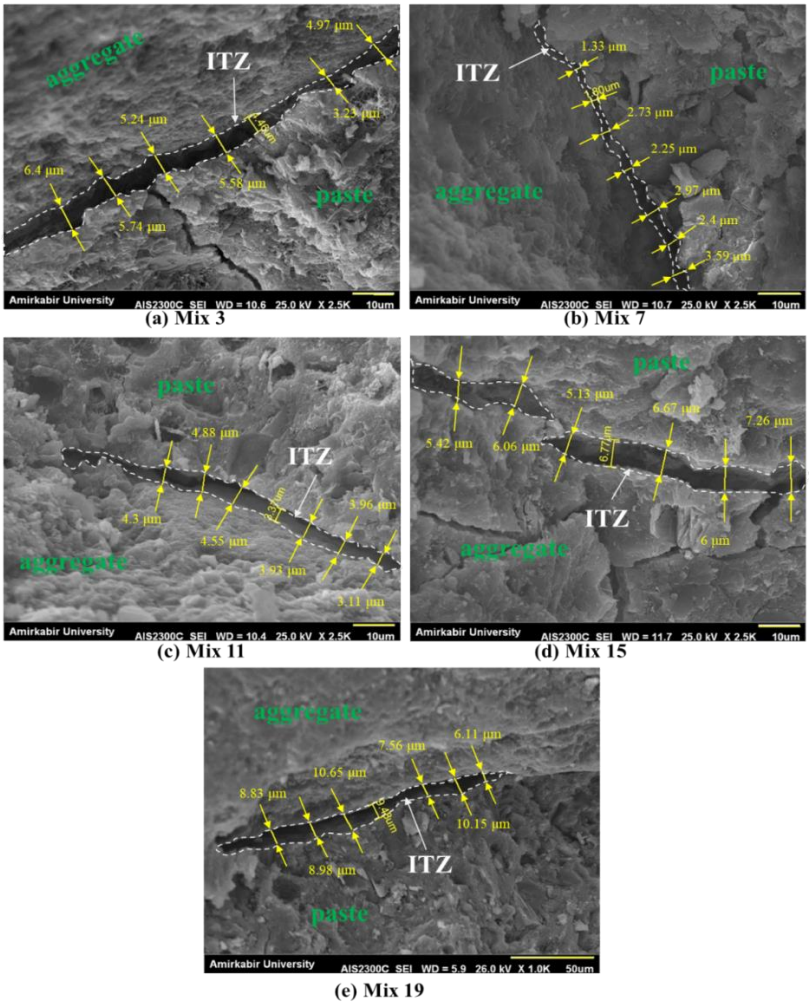

Figure 11. SEM images from specimens

5. Discussion

5.1. Relationship between BPN and Abrasion

Figure. 12 illustrates the inverse relationship between abrasion rate and British Pendulum Number (BPN) ($R^2 = 0.59$). This trend confirms that mixtures with lower initial BPN values experience higher abrasion rates, indicating greater surface wear and reduced resistance to polishing. The maximum aggregate size (MAS) plays a crucial role in moderating this relationship. Mixtures with initial BPN values greater than 65 (Table. 7)—which are considered acceptable for all pavement types according to relevant standards(Sabey, 1963)—correspond to MAS values of 19 mm, 25 mm, and 37.5 mm, and exhibit the lowest abrasion rates among the tested groups. Although the mixture with MAS = 37.5 mm showed lower abrasion rates, it was not considered favorable due to its unsatisfactory performance in the Box

test. In contrast, mixtures with MAS = 19 mm and 25 mm achieved both high initial BPNs and low abrasion rates, confirming their superior durability and texture retention. As initial BPN decreases, the abrasion rate increases, indicating a direct link between surface roughness and abrasion resistance. Overall, these findings confirm that gradation refinement—specifically, achieving a balanced combination of coarse and fine aggregates—significantly enhances both microtexture stability and abrasion resistance in concrete pavements.

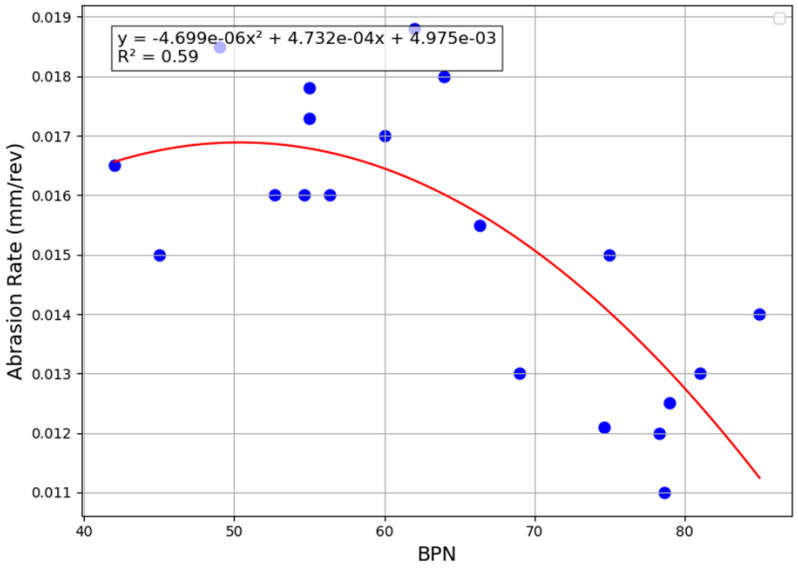

Figure 12. BPN vs Abrasion Rate (FTE as a categorical factor)

5.2. Influence of Packing Density and Layer Thickness on BPN

The BPN shows a positive correlation with aggregate packing density (Figure. 13) (R^2 = 0.913), indicating that denser aggregates enhance surface friction. Mixtures with MAS = 19 mm and 25 mm exhibit the highest BPN, suggesting that medium-sized aggregates offer the best balance between fine and coarse particles for optimal microtexture. In contrast, smaller aggregates (MAS = 9.5 mm and 12.5 mm) lead to smoother surfaces due to a higher proportion of fine particles, while larger aggregates (MAS = 37.5 mm) reduce microtexture due to compaction difficulties. Overall, increasing aggregate packing density improves microtexture, with the most favorable surface friction resulting from a combination of high packing density and intermediate aggregate sizes.

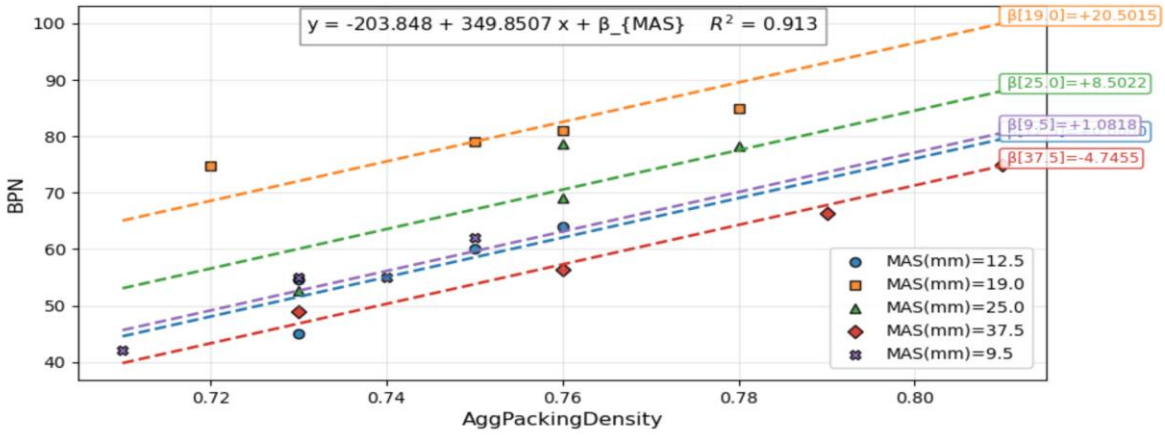

Figure 13. Aggregate Dry Packing density vs BPN (MAS as a categorical factor)

Figure. 14 demonstrates the expected smoothing effect of paste-film thickness (PFT) on surface microtexture. As suggested in Reference 2, the microtexture—which is responsible for surface roughness—is largely driven by the presence of fine aggregates in the mixture. These aggregates create roughness on the surface, resulting in a more textured microstructure that enhances frictional resistance. The paste film forms a layer around these aggregates, and as PFT increases, this layer smooths out the surface, reducing roughness and, consequently, diminishing the microtexture.

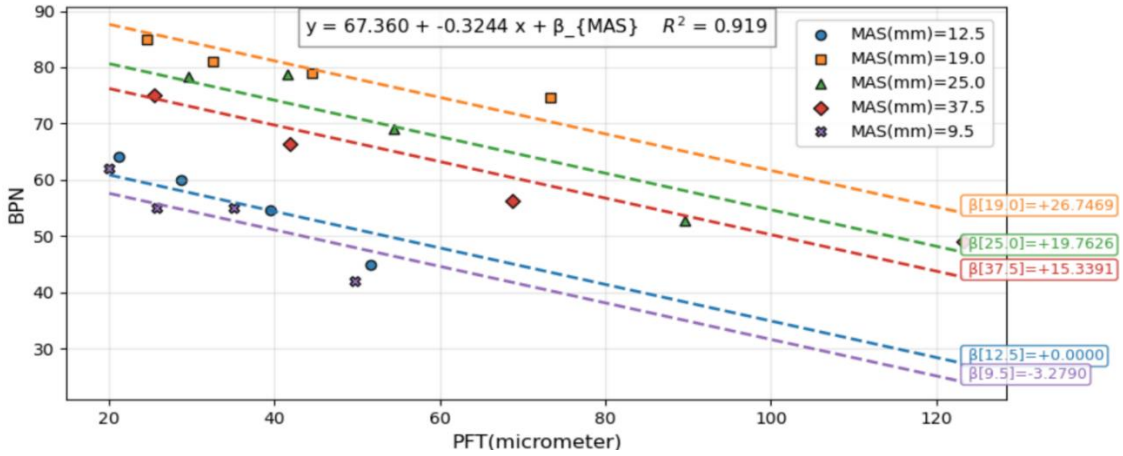

Figure 14. BPN vs PFT(µm) (MAS as a categorical factor)

Figure. 15 shows a positive correlation between BPN and mortar film thickness (MFT) (R^2 = 0.772), indicating that thicker mortar layers improve surface friction. This occurs because increased MFT introduces more fine particles into the surface layer, enhancing micro-asperities that contribute to friction. Mixtures with intermediate MAS (19 mm and 25 mm) achieve the highest BPN, suggesting that a balanced aggregate gradation provides the most favorable microtexture for skid resistance.

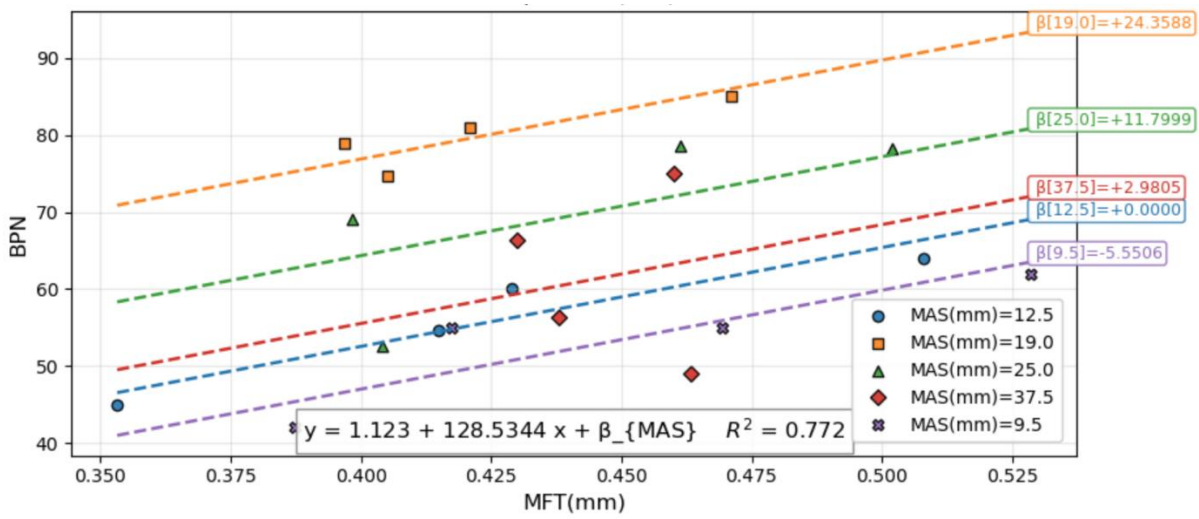

Figure 15. BPN vs MFT(mm) (MAS as a categorical factor)

Previous research has shown that increasing the packing density of aggregate particles can enhance both the fresh-state rheology and the hardened-state mechanical properties of concrete (Moini et al., 2015; Pradhan et al., 2019; Dingqiang et al., 2020; Vatannia, Kearsley and Mostert, 2020; Londero, Soares Klein and Mazer, 2021; Luansu et al., 2021; Abushama et al., 2023). However, the findings of this study indicate that the mixtures with

MAS values of 19 mm and 25 mm displayed the most favorable performance in terms of mechanical strength, skid resistance, and abrasion resistance. Notably, the corresponding values of concrete packing density (0.83–0.85based on Agg Packing density and the equation in Figure. 7) , PFT (24–73µm) , and MFT (0.40–0.50mm) for these mixtures were found to be in the mid-range of the overall ranges observed across all twenty mixtures. These results align with previous literature, as Kwan and colleagues (2018) (Kwan and Li, 2014) also recommended a PFT range of 20–60µm to optimize workability, which is consistent with the range we observed.

5.3. Influence of Microstructure on BPN

Figureures 16 illustrate the relationship between maximum aggregate size (MAS) and BPN, for mixes 3, 7, 11, 15, and 19, with MAS values of 37.5 mm, 25 mm, 19 mm, 12.5 mm, and 9.5 mm, respectively, following an FTE of 0.45. The data reveal a nonlinear relationship between MAS and these properties. BPN increases initially with MAS, peaking at MAS 25 mm and MAS 19 mm, before decreasing at larger sizes. This indicates that intermediate aggregate sizes provide an optimal balance for surface microtexture and aggregate-paste adhesion.

Microstructural analysis further supports these findings. Specifically, MAS 19 mm and 25 mm outperform other aggregate sizes in terms of average pore diameter and safe pore percentage. Additionally, the ITZ thickness is minimal at these intermediate MAS sizes, leading to a stronger aggregate–paste bond and improved structural integrity. The combination of these factors results in enhanced abrasion resistance and frictional properties, making MAS 19 mm and 25 mm the most efficient for durability and frictional resistance in concrete pavement applications.

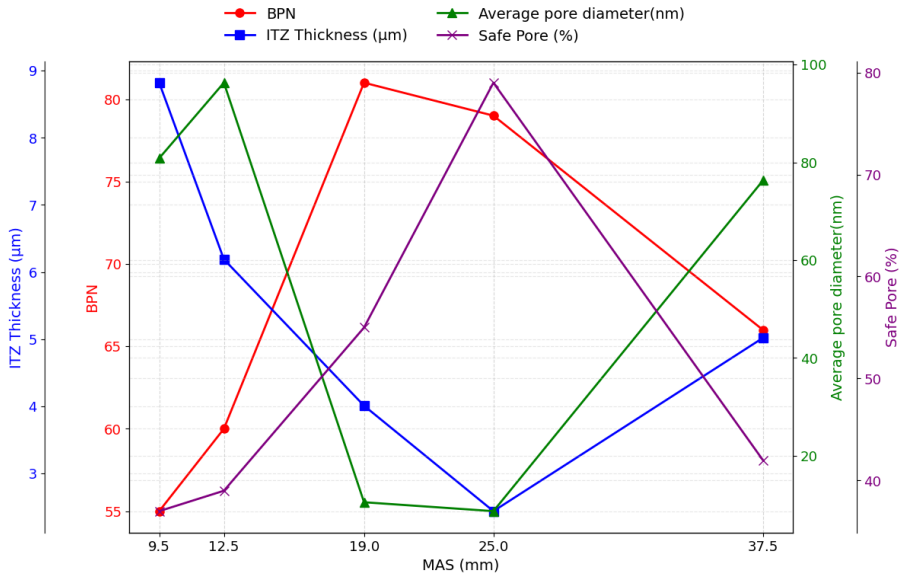

Figure 16. Effect of Microstructural Features and MAS on BPN

6. Conclusions

This study investigated the effects of MAS and gradation on fresh-state behavior, mechanical performance, surface characteristics, and pore structure in concrete mixtures designed for slip-form paving. The key findings, based on tests performed on 20 concrete mixtures, are summarized as follows:

- Mixtures with MAS of 37.5 mm met the slump flow criteria but exhibited inadequate shape retention and edge stability in the Box Test. These results suggest that slump values alone may not reliably reflect workability in slip-form paving applications, and that the

Box Test may better capture the necessary shape-holding behavior.

- The highest values of compressive strength and flexural strength were generally associated with MAS of 19 mm and 25 mm. Increasing FTE appeared to correspond with higher compressive strength Meanwhile, lower FTE values coincided with increased flexural strength, potentially due to effects related to interparticle contact and crack propagation patterns.
- Mixtures with MAS between 19 and 25 mm exhibited lower abrasion rates and BPN above the reference threshold of 65. These observations were consistent with the simultaneous impact of both MAS and gradation on surface abrasion and skid resistance characteristics.
- MIP results showed that mixes with intermediate MAS (19–25 mm) have lower total porosity, smaller average pore size, and a higher proportion of harmless pores. SEM confirmed that these mixes also have the thinnest, densest ITZ, which explains their superior durability and skid resistance.

For this study's conditions and materials, the effective window was: MAS 19–25 mm; packing density 0.83–0.85; PFT ≈24–73 μm; MFT ≈0.40–0.50 mm—achieving BPN ≥ 65, low abrasion rate, consistent Box Test performance, and improved mechanical properties.

This study shows that achieving safe wet friction and low abrasion in concrete pavements comes from jointly tuning MAS, gradation, and film/packing measures—rather than maximizing any single parameter.

It is recommended that future research extend beyond the present framework by examining different aggregate types, binder systems (e.g., high-SCM concretes), environmental exposure conditions, and field pavement sections in order to more rigorously assess the robustness of the proposed parameter windows.

7. References

– Abushama, W. J., Tamimi, A. K., Tabsh, S. W., El-Emam, M. M., Ibrahim, A., & Mohammed Ali, T. K. (2023). Influence of optimum particle packing on the macro and micro properties of sustainable concrete. Sustainability, 15. https://doi.org/10.3390/su151914331

– Alaskar, A., Alabduljabbar, H., Mustafa Mohamed, A., Alrshoudi, F., & Alyousef, R. (2021). Abrasion and skid resistance of concrete containing waste polypropylene fibers and palm oil fuel ash as pavement material. Construction and Building Materials, 282. https://doi.org/10.1016/j.conbuildmat.2021.122681

– ASTM International. (n.d.). ASTM C29/C29M-07: Standard test method for bulk density ("unit weight") and voids in aggregate. West Conshohocken, PA.

– ASTM International. (n.d.). ASTM C39/C39M: Standard test method for compressive strength of cylindrical concrete specimens. West Conshohocken, PA. (available at: www.astm.org)

– ASTM International. (n.d.). ASTM C138/C138M: Standard test method for density (unit weight), yield, and air content (gravimetric) of concrete. West Conshohocken, PA. (available at: www.astm.org)

– ASTM International. (n.d.). ASTM C150-07: Standard specification for Portland cement. West Conshohocken, PA. (available at: www.astm.org)

– ASTM International. (n.d.). ASTM C494/C494M-99a e1: Standard specification

for chemical admixtures for concrete. West Conshohocken, PA.

– ASTM International. (2015). ASTM C143/C143M-15a: Standard test method for slump of hydraulic-cement concrete. West Conshohocken, PA.

– ASTM International. (2016). ASTM C293/C293M-16: Test method for flexural strength of concrete (using simple beam with center-point loading). West Conshohocken, PA. https://doi.org/10.1520/C0293_C0293M-16

– ASTM International. (2008). ASTM E303-93(2008): Test method for measuring surface frictional properties using the British pendulum tester. West Conshohocken, PA. https://doi.org/10.1520/E0303-93R08

– Chu, S. H. (2019). Effect of paste volume on fresh and hardened properties of concrete. Construction and Building Materials, 218, 284–294. https://doi.org/10.1016/j.conbuildmat.2019.05.131

– Cook, M. D., Ley, M. T., & Ghaeezadah, A. (2014). A workability test for slip formed concrete pavements. Construction and Building Materials, 68, 376–383. https://doi.org/10.1016/j.conbuildmat.2014.06.087

– Dingqiang, F., Rui, Y., Zhonghe, S., Chunfeng, W., Jinnan, W., & Qiqi, S. (2020). A novel approach for developing a green ultra-high performance concrete (UHPC) with advanced particles packing meso-structure. Construction and Building Materials, 265. https://doi.org/10.1016/j.conbuildmat.2020.120339

– EN 1338. (n.d.). Concrete paving blocks – Requirements and test methods. Wide wheel abrasion test.

– Fattouh, M. S., Abouelnour, M. A., Mahmoud, A. A., Fathy, I. N., El Sayed, A. F., Elhameed, S. A., & Nabil, I. M. (2025). Impact of modified aggregate gradation on the workability, mechanical, microstructural and radiation shielding properties of recycled aggregate concrete. Scientific Reports, 15. https://doi.org/10.1038/s41598-025-02655-y

– Ghoddousi, P., Shirzadi Javid, A. A., & Sobhani, J. (2014). Effects of particle packing density on the stability and rheology of self-consolidating concrete containing mineral admixtures. Construction and Building Materials, 53, 102–109. https://doi.org/10.1016/j.conbuildmat.2013.11.076

– Hall, J. W., Smith, K. L., Titus-Glover, L., Wambold, J. C., Yager, T. J., & Rado, Z. (2009). Web-only document 108: Guide for pavement friction. National Cooperative Highway Research Program (NCHRP).

– Kane, M., & Edmondson, V. (2022). Tire/road friction prediction: Introducing a simplified numerical tool based on contact modelling. Vehicle System Dynamics, 60, 770–789. https://doi.org/10.1080/00423114.2020.1832696

– Koehler, E. P., & Fowler, D. W. (n.d.). ICAR mixture proportioning procedure for self-consolidating concrete. ICAR, University of Texas at Austin. Retrieved from www.icar.utexas.edu

– Kwan, A. K. H., & Li, L. G. (2014). Combined effects of water film, paste film and mortar film thicknesses on fresh

properties of concrete. Construction and Building Materials, 50, 598–608. https://doi.org/10.1016/j.conbuildmat.2013.10.014

– Lashari, A. R., Ali, Y., Buller, A. S., & Memon, N. A. (2023). Effects of partial replacement of fine aggregates with crumb rubber on skid resistance and mechanical properties of cement concrete pavements. International Journal of Pavement Engineering, 24. https://doi.org/10.1080/10298436.2022.2077940

– Li, L. G. (2013). Roles of water, paste and mortar film thicknesses in performance of mortar and concrete (Doctoral thesis).

– Li, L. G., & Kwan, A. K. H. (2014). Packing density of concrete mix under dry and wet conditions. Powder Technology, 253, 514–521. https://doi.org/10.1016/j.powtec.2013.12.020Li, Z. (2011). Advanced Concrete Technology. John Wiley & Sons.

– Liu, Q., Guo, L., Miao, J., & Jia, D. (2025). A novel nonlinear model for estimating ideal packing density of mixtures. Scientific Reports, 15. https://doi.org/10.1038/s41598-025-87856-1

– Londero, C., Soares Klein, N., & Mazer, W. (2021). Study of low-cement concrete mix-design through particle packing techniques. [Open-access article]. Retrieved from https://www.elsevier.com/open-access/userlicense/1.0/

– Luansu, W., Wenqiang, Z., Hao, P., Kai, L., Wenhua, Z., & Wei, S. (2021). Rational design of lightweight cementitious composites with reinforced mechanical property and thermal insulation: Particle packing, hot pressing method, and microstructural mechanisms. Composites Part B: Engineering, 226.

– Mamirov, M. (n.d.). Using theoretical and experimental particle packing for aggregate gradation optimization to reduce cement content in pavement concrete mixtures. Retrieved from https://digitalcommons.unl.edu/civilengdiss

– Meddah, M. S., Zitouni, S., & Belâabes, S. (2010). Effect of content and particle size distribution of coarse aggregate on the compressive strength of concrete. Construction and Building Materials, 24, 505–512. https://doi.org/10.1016/j.conbuildmat.2009.10.009

– Moini, M., Flores-Vivian, I., Amirjanov, A., & Sobolev, K. (2015). The optimization of aggregate blends for sustainable low cement concrete. Construction and Building Materials, 93, 627–634. https://doi.org/10.1016/j.conbuildmat.2015.06.019

– Nejad, F. M., Karimi, N., & Zakeri, H. (2016). Automatic image acquisition with knowledge-based approach for multi-directional determination of skid resistance of pavements. Automation in Construction, 71, 414–429. https://doi.org/10.1016/j.autcon.2016.08.003

– Pei, Q., Zhong, Y., Wang, S., Zhang, L., & Lai, Y. (2025). Interlayer bonding shear performance and constitutive model of 3DPC with different fine aggregate gradations. Construction and Building Materials, 486, 142024. https://doi.org/10.1016/J.CONBUILDMAT.2025.142024

– Pradhan, S., Tiwari, B. R., Kumar, S., & Barai, S. V. (2019). Comparative LCA of recycled and natural aggregate concrete using particle packing method and conventional method of design mix. Journal of Cleaner Production, 228, 679–691. https://doi.org/10.1016/j.jclepro.2019.04.328

– Road Research Laboratory. (1969). Instructions for using the portable skid-resistance tester. HM Stationery Office, London.

– Schmidt, M. (2004). Ultra high performance concrete (UHPC). In Proceedings of the International Symposium on Ultra High Performance Concrete, Kassel, Germany, September 13–15, 2004.

– Senthilvelan, J., Izuo, H., Endo, T., & Ueno, A. (2024). Relationship between surface material indices and skid resistance of concrete pavement. Construction and Building Materials, 449. https://doi.org/10.1016/j.conbuildmat.2024.138435

– Sherwood, J. A. (2011). Effects of concrete mixture designs on skid numbers. In Proceedings of the 8th International Conference on Managing Pavement Assets. Federal Highway Administration, Intervial Chile, CAF–Banco de Desarrollo de América Latina.

– Sun, Z., Yang, S., Hang, M., Wang, J., & Yang, T. (2022). Optimization design of ultrahigh-performance concrete based on interaction analysis of multiple factors. Case Studies in Construction Materials, 16, e00858. https://doi.org/10.1016/j.cscm.2021.e00858

– Sun, Z., Xiong, J., Cao, S., Zhu, J., Jia, X., Hu, Z., & Liu, K. (2023). Effect of different fine aggregate characteristics on fracture toughness and microstructure of sand concrete. Materials, 16, 2080. https://doi.org/10.3390/ma16052080

– Taylor, P., Wang, X., & Yurdakul, E. (2018). An innovative approach to concrete mixture proportioning. ACI Materials Journal, 115, 749–759. https://doi.org/10.14359/51702351

– Vatannia, S., Kearsley, E., & Mostert, D. (2020). Development of economic, practical and green ultra-high performance fiber reinforced concrete verified by particle packing model. Case Studies in Construction Materials, 13, e00415. https://doi.org/10.1016/j.cscm.2020.e00415

– Wang, Y., Zhang, W., Wang, J., Huang, R., Lou, G., & Luo, S. (2024). Effects of coarse aggregate size on thickness and micro-properties of ITZ and the mechanical properties of concrete. Cement and Concrete Composites, 154. https://doi.org/10.1016/j.cemconcomp.2024.105777

– Wasilewska, M., Gardziejczyk, W., & Gierasimiuk, P. (2018). Effect of aggregate graining compositions on skid resistance of exposed aggregate concrete pavement. In IOP Conference Series: Materials Science and Engineering, 356, 012001. https://doi.org/10.1088/1757-899X/356/1/012001

– Wong, H. H. C., & Kwan, A. K. H. (2008). Packing density of cementitious materials: Part 1 – Measurement using a wet packing method. Materials and Structures, 41, 689–701. https://doi.org/10.1617/s11527-007-9274-5

– Wong, H. H. C., & Kwan, A. K. H. (2005). Packing density: A key concept for mix design of high performance concrete. In Proceedings of the Materials Science and Technology in Engineering Conference. HKIE Materials Division, Hong Kong, 1–15.

– Xiao, J., Lv, Z., Duan, Z., & Zhang, C. (2023). Pore structure characteristics, modulation and its effect on concrete properties: A review. Construction and Building Materials, 397. https://doi.org/10.1016/j.conbuildmat.2023.132430

– Yurdakul, E., Taylor, P. C., Ceylan, H., & Bektas, F. (2013). Effect of paste-to-voids volume ratio on the performance of concrete mixtures. Journal of Materials in Civil Engineering, 25, 1840–1851. https://doi.org/10.1061/(ASCE)MT.1943-5533.0000728

– Zhao, W., Zhang, J., Lai, J., Shi, X., & Xu, Z. (2023). Skid resistance of cement concrete pavement in highway tunnel: A review. Construction and Building Materials, 406, 133235. https://doi.org/10.1016/j.conbuildmat.2023.133235